Microstructure and magnetic properties of 2:17-type Sm-Co permanent magnets according to heat treatment conditions

Seungil Park[1], Seunghan Kim[1], Kyoung-Hoon Bae[2], and Tae-Hoon Kim[1*]
[1]Department of Materials Science & Engineering, Chonnam National University, Gwangju, Republic of Korea
[2]R&D Center of Star Group Co. Ltd, Daegu, Republic of Korea

Sm-Co magnets are attracting attention, especially in the military equipment and automobile market due to their high-temperature magnetic properties such as coercivity. Sm has an approximately three times lower price compared to Nd of Nd magnets which have been widely used. The ease of securing raw materials and its potential for high-temperature application make Sm-Co magnets highly valuable for research. In Sm2Co17 magnets, the supersaturated phase is formed by solution treatment after the sintering. Then it undergoes a two-step heat treatment process consisting of isothermal heat treatment at around 850℃ for about 20 hours, followed by annealing at around 400℃ for about 10 hours. By forming a cell structure through the formation of SmCo5 boundary phase covering the Sm2Co17 main phase, high coercivity can be achieved. In this study, we find the optimal process conditions by investigating microstructures and magnetic properties with different heat treatment conditions including solution treatment, 1st isothermal aging, and 2nd isothermal aging step. We investigate the correlation between magnetic properties and microstructure such as the formation of the main phase, boundary phase, and z-phase, continuity, and distribution of solute atoms.

Development of Sm-Fe-N sintered magnet though low oxygen powder metallurgy process

Yusuke HIRAYAMA
(National Institute of Advanced Industrial Science and Technology)

As post-neodymium magnets, Sm-based ferromagnetic compounds have higher potential as permanent magnets than $Nd_2Fe_{14}B$. Examples of Sm-based compounds that have been reported so far include $Sm_2Fe_{17}N_3$ with Th_2Zn_{17} structurte[1,2], SmZrFeCoTi with $ThMn_{12}$ structure[3, 4], and $SmZr(FeCo)_{10}N_x$ with $TbCu_7$ structure[5]. However, they have not been able to surpass neodymium magnets because the processes that can bring out their high potential are not yet mature. Although it is possible to produce anisotropic powder from the stable phase of $Sm_2Fe_{17}N_3$, the decomposition temperature is relatively low at 620°C. Therefore, a dense sintered body with sufficient density is challenging. In addition, as for the metastable phase of $SmZr(FeCo)_{10}N_x$, the process for obtaining anisotropic powder has not been established. In response to these challenges, we have developed improved/new processes for producing anisotropic magnets. In this work, various fine powder synthesis processes and their sintering processes will be introduced.

1. Pulverization process: In order to improve the magnetic properties of the $Sm_2Fe_{17}N_3$ compound as a permanent magnet material, especially its coercivity, fine powder is necessary. The properties have been improved using ball mill and jet mill processes. In the jet mill process, high properties have been obtained by controlling the crushing damage and the particle size distribution appropriately [6].
2. Physical/chemical process: The above-mentioned pulverization method cannot completely remove the damage to the particle surface during crushing. Therefore, by using oxide powder as the raw material and reducing it with hydrogen and Ca metal, it is possible to obtain Sm-Fe alloys with high crystallinity up to the particle surface. As a result, submicron-sized $Sm_2Fe_{17}N_3$ particles with an extremely high coercivity of 3.2 T at room temperature have been successfully synthesized [7]. Recently, the thermal plasma method has been used to synthesize nano-sized single crystal particles with an average particle size of 100 nm or less. In particular, metastable anisotropic Sm-Fe-N powder has been successfully synthesized using both the improved reduction diffusion and thermal plasma process [8].
3. Sintering process: As mentioned above, the $Sm_2Fe_{17}N_3$ compound decomposes at 620°C, making it impossible to sinter at high temperatures, and it is difficult to obtain a dense sintered body. In addition, there was a problem of a significant decrease in coercivity during sintering, making it difficult to bring out the properties of the compound. We investigated the cause of the decrease in coercivity for this difficult-to-sinter compound, which is surface oxidation of the powder, and succeeded in creating a process in which there is no decrease in coercivity during sintering by removing as much oxygen as possible from the pulverization process [6]. In addition, we have discovered a sintering aid that does not decrease coercivity during sintering even if the powder surface is oxidized [9].

<u>Reference</u>

[1] T. Iriyama et al., Magnetics, IEEE Transactions on, 28, 2326-2331, (1992).
[2] J.M.D. Coey et al., Journal of Applied Physics, 69, 3007-3010, (1991).
[3] P. Tozman et al., Applied Physics Express, 15, 045505, (2022).
[4] P. Tozman et al., Scripta Mater., 194 (2021).
[5] S. Sakurada et al., J. Appl. Phys., 79, 4611-4613, (1996).
[6] K. Takagi et al., Science and Technology of Advanced Materials, 22, 150-159, (2021).
[7] S. Okada et al., Journal of Alloys and Compounds, 960, 170726, (2023).
[8] S. Okada et al., Journal of Rare Earths, 40, 1126-1133, (2022).
[9] K. Otogawa et al., J. Alloy. Compd., 746, 19‑26, (2018).

Extracting the phase information about demagnetization field within thin-foiled Nd-Fe-B magnets using electron holography

S. Lee[1,2], A. Sato[2], T. Tamaoka[2], K. Yubuta[2], M. Auchi[2], T. Sasaki[3], T. Ohkubo[3], and Y. Murakami[2]
[1]Korea Institute of Materials Science (KIMS), Changwon, 51508, Korea
[2]Kyushu University, Fukuoka, 819-0395, Japan
[3]National Institute for Materials Science, Tsukuba, 305-0047, Japan

Nd-Fe-B based permanent magnet has been used in many applications such as traction motors in electric/hybrid vehicles because of the high anisotropy field and saturation magnetization of the $Nd_2Fe_{14}B$ matrix. The automobile industry has required further improved coercivity (H_c), which is a measure of the critical field to induce undesired magnetization reversal, to miniaturize the traction motors of electric/hybrid vehicles and increase their performance. However, the coercivity of a sintered Nd-Fe-B magnet commercially used is smaller than the theoretical upper limit (less than 20% of the anisotropy field) of the $Nd_2Fe_{14}B$ phase. For understanding of the coercivity mechanism in the sintered Nd-Fe-B magnet, observation of the demagnetization field (H_d) within crystal grains is essential, as H_d is relevant to undesired magnetization reversal[1)]. However, direct observation of H_d remains to be challenge because the lack of experimental tools. Although electron holography has been widely used in magnetic domain observations for a thin-foiled specimen through the analysis of the phase shift of incident electron waves, this method only provides the information about magnetic flux density (B), which is the summation of magnetization (M), stray magnetic field outside of the specimen (H_s), and H_d inside of the specimen[2)]. Therefore, in this study, we proposed a method to extract the H_d information from electron holography observation. [3)]

To reduce the undesired sources for the phase shift, *i.e.*, M and H_s, the M contribution was determined by the orientation analysis of the c-axis (*i.e.*, easy magnetization axis) in the $Nd_2Fe_{14}B$ grain. The H_s contribution was calculated in three dimensions using a magnetic-field simulator when the specimen shape, specimen thickness, and the c-axis direction are uncovered by electron microscopy observations. Following this procedure, the mapping of H_d was attained for a single-crystalline $Nd_2Fe_{14}B$ foil, as shown in Fig. 1. The plot of mapping H_d was in a good agreement with the predictions from both classical electromagnetism and micromagnetic theory. The results show the validity of this method to examine the demagnetization field, which will be addressed in the session.

Reference
1) J. Li et al., Acta. Mater. **161** (2018) 171
2) A. Tonomura, Electron holography. Second edit, Springer, Heidelberg (1999)
3) S. Lee et al., Appl. Microsc., **54** (2024) 4.

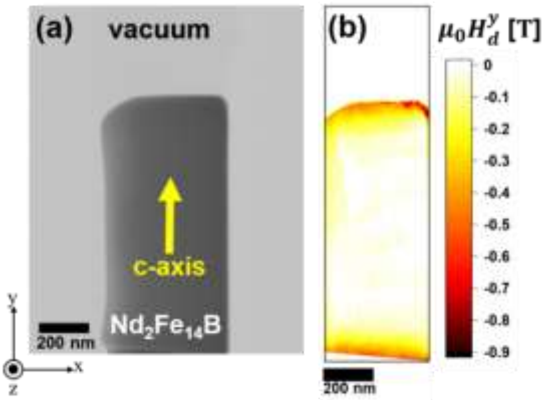

Fig. 1 (a) TEM image of a $Nd_2Fe_{14}B$ thin-foiled specimen, magnetized in the direction of yellow arrow. (b) Mapping of the y component of demagnetization field H_d within the specimen. [3)]

Magnetic properties and Microstructure of $TbCu_7$-type Sm-Fe-Co-Nb-B alloy

M. Matsuura[1], Y. Hinata[1*], N. Kurokawa[1**], S. Sakurada[2], N. Tezuka[1], and S. Sugimoto[1]

[1] Department of Materials Science, Graduate School of Engineering, Tohoku University, Sendai 980-8579, Japan.

[2] Nano Materials & Frontier Research Laboratories, Corporate Research & Development Center, Toshiba Corporation, Kawasaki, 212-8582, Japan.

$TbCu_7$-type Sm-Fe phase is one of the promising candidates for high performance magnets. Dr. Katter et al.[1)] reported that the metastable $TbCu_7$-type Sm-Fe phase in rapidly quenched melt-spun ribbons and showed that the magnetic properties of $TbCu_7$-type Sm-Fe alloy were improved by nitriding. After that, Dr. Sakurada et al.[2)], reported excellent magnetic properties including high saturation magnetization and anisotropy field of 1.70 T and 6.2 MA/m, respectively, for Sm-Zr-Fe-Co-N alloy. $TbCu_7$-type Sm-Fe-Co-Nb-B alloy was firstly reported by Dr. Mochizuki et al.[3)]. They reported amorphous ribbon was obtained with relatively slow roll velocity, and $TbCu_7$-type phase formed by subsequent annealing with relatively high coercivity without nitriding. Recently, our group also studied the Sm-Fe-Co-Nb-B alloy system, and obtained high coercivity ribbon of 695 kA/m and high thermal stability resin-bonded magnet[4)]. Furthermore, our group have attempted to develop alternative process to prepare $TbCu_7$-type Sm-Fe-Co-Nb-B powder, directly, using gas atomization[5)]. In this study, the relationship between composition, microstructure and magnetic properties of Sm-Fe-Co-Nb-B alloy are presented.

Sm-Fe-Co-Nb-B alloys were subjected to induction melting followed by melt spinning and gas atomizing to obtain quenched ribbon and quenched powder, respectively. The as-spun ribbons and powders were heat treated at 600-675 °C for 1–25 h. The magnetic properties were evaluated by VSM with maximum applied field of 1.6 MAm^{-1} after magnetized by a pulsed magnetic field of 6.4 MAm^{-1}. The anisotropy field was estimated using the law of approach to ferromagnetic saturation (LAS) method with a maximum applied magnetic field of 4.8 MAm^{-1}. The saturation magnetization was also measured under an applied magnetic field of 4.8 MAm^{-1}. Crystal structure was measured by X-ray diffraction (XRD). Microstructure was observed by field emission scanning electron microscopy (FE-SEM) and transmission electron microscopy (FE-TEM).

Sm-Fe-Co-Nb-B amorphous ribbons were annealed under optimized conditions, and investigated coercivity and anisotropy field. Coercivity depends on Sm, Nb and B content, and it also related to its anisotropy field. It is suggested that the increasing anisotropy field related to additional element contributes to high coercivity without nitriding. Increasing Nb and B contents facilitated amorphous forming in the Sm-Fe-Co-Nb-B alloy system, and spherical shaped Sm-Fe-Co-Nb-B powders, which consists amorphous phase as main phase, was obtained by gas atomizing. Then, after annealing at 650 or 675 °C, coercivity increased and reached around 300 kA/m with crystallization of $TbCu_7$-type phase. The optimum annealing temperature for gas atomized powder was higher than that for amorphous ribbons because crystallization temperature of $TbCu_7$-type phase increased with increasing Nb and B content.

Acknowledgement

This study was partially supported by a project, the New Energy and Industrial Technology Development Organization (NEDO), Japan (JPNP20019)

Reference

1) M. Katter, et al., *J. Appl. Phys.,* **70** (1991) 3118-3196.
2) S. Sakurada, et al., *J. Appj. Phys.*, **79** (1996) 4611-4613.
3) M. Mochizuki, et al., Proceedings of the Seventh International Workshop on Rare Earth Magnets and Their Applications, Newark, Delaware, USA, (2002), 401-408.
4) N. Kurokawa, et al., *J. Magn. Magn. Mater.,* **556** (2022) 169414 1-9.
5) Y. Hinata, et al., Collected Abstracts of the 2023 Autumn Meeting of the Japan Inst. Metals, (2023) S7.9.

[*]Graduate Student, Tohoku Univ., Present address: NSK Ltd. [**]Graduate Student, Tohoku Univ., Present address: Toshiba Co.

A novel guide to development of grain boundary diffusion process for high-performance Nd-Fe-B permanent magnets

Tae-Hoon Kim*

[1]*Powder and Ceramics Division, Korea Institute of Materials Science (KIMS), 797 Changwondaero, Changwon-city, 51508, South Korea.*

The grain boundary diffusion process (GBDP), which is firstly developed by Hirota *et al*., is the most effective industrial process for obtaining high-coercivity above 2.5 T in Nd-Fe-B permanent magnets with a minimum use of high-cost rare-earths (Tb, Dy, or Pr) that is essential for the coercivity enhancement [1]. Since the GBDP was developed in 2006, most researchers have focused on increasing the GBD depth of the diffusing elements such as Dy, Tb, or Pr [2]. To increase the grain boundary diffusivity of diffusing elements, only the GBDP temperature/time or melting temperature of diffusing elements, which is involved in the kinetics of GBD, have been considered so far [2]. However, as it was recently revealed by Kim *et al*. that the most dominant formation mechanism of the high-anisotropy (HA)-shell is the chemically induced liquid film migration (CILFM) [3], a new view-point in increasing the GBD depth of diffusing elements and improving the coercivity can be proposed, *i.e.*, the next-generation GBDP should be developed to suppress the CILFM because the CILFM consumes the diffusing elements and induces the unnecessary grain growth. Thus, in this presentation, we report a detailed microstructural character of the GBDP magnets that is clearly identified so far. Based on the formation mechanism of HA-shell including the CILFM, a novel guide to further improve the GBDP depth of diffusing materials and coercivity of GBDP magnets will be proposed.

Reference
1) Hirota et al., IEEE Trans. Magn., 42 (2006) 2909-2911.
2) K. Loewe et al., Acta Mater., 83 (2015) 248-255.
3) T. H. Kim et al., Scr. Mater., 178 (2020) 433-437.

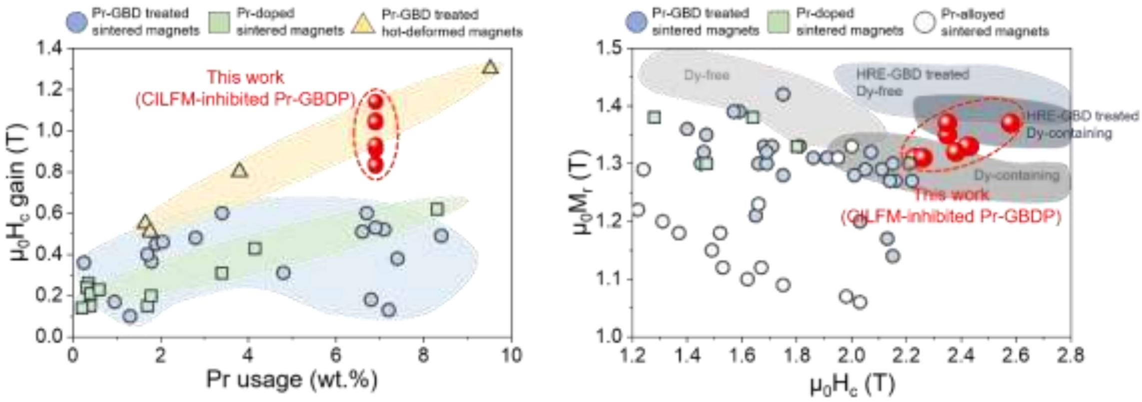

Figure 1. (Left side) μ_0H_c gain by Pr-GBDP or Pr-doping as a function of Pr usage, which are reported in the literatures [##]. The blue circles and yellow triangles correspond to the Pr-GBD treated sintered and hot-deformed magnets, respectively, and the green squares correspond to the Pr-doped sintered magnets. (Right side) μ_0H_c and μ_0M_r of Pr-GBD treated (blue circles), Pr-doped (green squares), and Pr-Fe-B (white circles) sintered magnets. The hard magnetic properties for commercial base magnets and HRE-GBD treated magnets are also displayed.

Engineering β-W Alloys for Highly Efficient Spin-Orbit Torque Switching

Young Keun Kim[1], Jiyoung Lee[1], Quynh Anh T. Nguyen[2], and Sonny H. Rhim[2]

[1] Department of Materials Science and Engineering, Korea University, Seoul 02841, Republic of Korea
[2] Department of Physics, University of Ulsan, Ulsan 44610, Republic of Korea

Spin-orbit torque (SOT) induced magnetization switching is a complex technology currently of great interest for various spintronic applications. It can potentially revolutionize nonvolatile embedded memory, such as magnetic random access memory (MRAM), logic devices, and true random number generators. These devices require a few nanometer-thick materials with perpendicular magnetic anisotropy (PMA) for high bit density, significant SOT efficiency to reduce writing current and energy consumption, and external field-free switching. Above all, the SOT materials must be semiconductor fabrication friendly. However, only a few materials sets and their heterostructures fulfill the requirements. In our recent research, we have faced the challenge of exploring various alloying elements, including Ta [1], N [2], V [3], Si [4], and Ti, into the β-phase W matrix as a spin current generating layer with enhanced SOT efficiencies. We employ the first-principles energy band calculations to narrow down the compositional ranges where we can get high spin Hall conductivity (σ_{SH}) values. This study presents the theoretical and experimental investigations on the σ_{SH} of Ti-alloyed β-W structures. The first-principles calculation predicts the highest σ_{SH} value of -1461 ($\hbar$/e) S/cm at Ti 12.5 at%. We fabricate β-W-Ti (*x* at%) 5/CoFeB 0.9/MgO 1 (in nm) heterojunctions with various Ti compositions to confirm the above result experimentally. The heterojunction with β-W-Ti 11.5 at% exhibits an enhanced damping-like SOT efficiency of 0.54 with longitudinal resistivity of 149.7 μΩ·cm. The current density (J_c) reaches as low as 15.5 MA/cm^2. We also demonstrate the SOT switching at operating temperatures ranging from -55 to +150^{o}C, required for aerospace and automobile memory applications.

References

1) I. H. Cha, T. Kim, Y. J. Kim, G. W. Kim, Y. K. Kim, J. Alloys Compd. 823 (2020) 153744.
2) Y. J. Kim, M. H. Lee, G. W. Kim, T. Kim, I. H. Cha, Q. A. T. Nguyen, S. H. Rhim, Y. K. Kim, Acta Mater. 200 (2020) 551–558.
3) G. W. Kim, D. D. Cuong, Y. J. Kim, I. H. Cha, T. Kim, M. Lee, O. Lee, H. Baik, S. C. Hong, S. H. Rhim, Y. K. Kim, NPG Asia Mater. 13 (2021) 60.
4) T. Kim, Q. A. T. Nguyen, G. W. Kim, M. H. Lee, S. I. Yoon, S. H. Rhim, Y. K. Kim, Appl. Surf. Sci. 609 (2023) 155352.

Spin and orbit torques in artificial alloy thin films and heterostructures

Zhenchao Wen, Tadakatsu Ohkubo, Hiroaki Sukegawa, and Seiji Mitani
National Institute for Materials Science (NIMS), Tsukuba 305-0047, Japan

Spin and orbital torques have become crucial for fast and energy efficient magnetization switching in spintronic devices, such as spin–orbit torque (SOT) magneto-resistive random access memories (MRAMs). When a longitudinal charge current passed through a nonmagnetic thin film, spin and orbital currents arise along the transverse direction due to the spin Hall effect (SHE) and orbital Hall effect (OHE), respectively, and can exert torques on the adjacent ferromagnetic layer, as schematically illustrated in Fig.1. Large spin and orbital torque efficiencies are essential for the development of SOT-MRAMs and related technologies. Materials such as topological insulators and heavy metals exhibit significant spin Hall efficiencies due to their large spin orbit coupling, while light metals are reported to possess strong orbital Hall effects. In this talk, we will present enhanced spin and orbital torque efficiencies in well-engineered artificial heterostructures and alloy thin films, including topological insulator BiSb/Ti/NiFe heterostructures [1] and nonequilibrium RuMo alloy thin films [2].

All the thin films were deposited on sapphire *c*-plane substrates using an ultra-high vacuum magnetron sputtering system. The structural characteristics of these films were analyzed using reflection high energy electron diffraction, X-ray diffraction, atomic force microscopy, and high-angle annular dark-field scanning transmission electron microscopy. Coplanar waveguide devices were fabricated using conventional UV lithography to assess spin and orbital torque efficiencies via spin-torque ferromagnetic resonance techniques.

We investigated the effect of the Ti insertion layer on the torque efficiency of two series of samples, BiSb/NiFe and BiSb/Ti/NiFe, under as-deposited, room-temperature aging and annealing conditions. Samples with the Ti layer showed a multifold increase in torque efficiency compared to those without Ti insertion. Atomic resolution microstructural analysis clearly illustrates the interfacial chemistry where Ti effectively prevents the interdiffusion of Ni and Sb. This interfacial chemistry near Ti at the interface of BiSb/NiFe significantly enhances torque efficiency. On the other hand, epitaxial thin films of a fully nonequilibrium hcp-$Ru_{50}Mo_{50}$(0001) were prepared as a chemically disordered alloy with an expected negligible intrinsic SHE. Structural analysis confirmed epitaxial growth and atomic-scale alloying of the thin films. Unlike the modest torque efficiency (~0.4%) observed for $Ru_{50}Mo_{50}$/CoFeB, the torque efficiency for the $Ru_{50}Mo_{50}$/Ni bilayers reached approximately 30% with a long-range relaxation length. The observed large variation in torque efficiency with the ferromagnetic layer could be attributed to the OHE. Interestingly, a small torque efficiency was observed for Ru/Ni, indicating that the nonequilibrium $Ru_{50}Mo_{50}$ composition enhances the OHE. Furthermore, inserting a Ru layer between the $Ru_{50}Mo_{50}$ and Ni layers maintains and improves torque efficiency, indicating orbital transport through Ru. These results not only show the significance of artificially engineered heterostructures and nanoalloy thin films for potential applications in spin and orbital torque technologies, but also contribute to the understanding of the intricate relationships between nanostructures and spin-orbitronics.

This work was partially supported by JST CREST (JPMJCR19J4) and JSPS KAKENHI (22H04966).

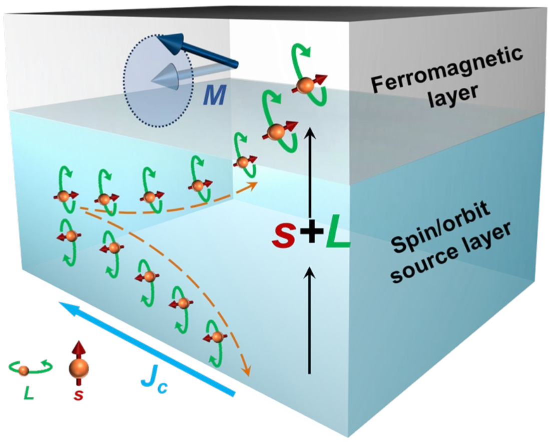

Fig. 1. Illustration of the spin and orbital Hall effects and interaction with the magnetic moment of the adjacent ferromagnetic layer.

References

1) T. Manoj, Z. Wen *et al.*, ACS Appl. Electron. Mater. **6**, 4269 (2024).
2) K. Tang, C. He, Z. Wen *et al.*, APL Mater. **12**, 031131 (2024).

Electrically Induced Phase Transition of Interlayer Magnetic Coupling in the $Fe_{5-x}GeTe_2$ with Current In-Plane Geometry

Sanghoon Kim[1]

[1]*University of Ulsan, Ulsan, 44610, Republic of Korea*

In this presentation, microscopic structures and magnetic properties of the $Fe_{5-x}GeTe_2$ single crystal, recently discovered as a promising van der Waals (vdW) ferromagnet, are introduced. Our study demonstrates a new way of the magnetization control of the vdW magnets via the electrical control of the interlayer coupling from ferromagnetic (FM)-to-antiferromagnetic (AFM). The current-induced phase transition results in drastically enhanced magnetoresistance from 5% to 170% with current in-plane geometry. This observation is fundamentally different from other conventional ways such as spin torque effects and gate voltage effects.
This study will provide essential information to understand the complex magnetic properties and the origin of the new vdW ferromagnet, $Fe_{5-x}GeTe_2$ for future topology-based spin devices.

Superconducting proximity effect in a $NbSe_2$/graphene van der Waals junction

Rai Moriya and Tomoki Machida
Institute of Industrial Science, University of Tokyo, Tokyo 153–8505, Japan

The proximity effect between a superconductor and graphene across the van der Waals interface is a subject of interest. Previously, we reported that the exfoliated surface of the layered material superconductor $NbSe_2$ provides an atomically flat and inert surface that can be useful as a source of supercurrent [1]. This study investigates the transport properties of van der Waals (vdW) junctions between layered $NbSe_2$ superconductors and graphene. A superconductor/graphene (S/G) vdW junction was fabricated by the dry transfer of freshly exfoliated $NbSe_2$ flakes onto a graphene surface. This vdW junction provides a transparent superconductor/graphene contact, as well as metal-induced doping in the graphene layer underneath, thereby facilitating vdW coupling-induced superconductivity in the graphene under the $NbSe_2$ layer. The $NbSe_2$/superconducting graphene (Sc-graphene)/graphene structure causes the differential resistance of the vdW junction to exhibit a zero-bias dip and multiple peaks at a larger bias. These features can be explained by the coexistence of two different S/G interfaces in the device: the lateral Sc-graphene/graphene and vertical $NbSe_2$/Sc-graphene interfaces [2), 3)]. A proximity-induced superconducting gap Δ_i in the Sc-graphene is detected by Andreev reflection at the lateral Sc-graphene/graphene junction, and the determined Δ_i =0.05−0.06 meV.

Reference

1) N. Yabuki, R. Moriya, M. Arai, Y. Sata, S. Morikawa, S. Masubuchi, and T. Machida, Nat. Commun. **7**, 10616 (2016).
2) R. Moriya, N. Yabuki, and T. Machida, Phys. Rev. B **101**, 054503 (2020).
3) Y. Sata, R. Moriya, N. Yabuki, S. Masubuchi, and T. Machida, Phys. Rev. B **98**, 035422 (2018).

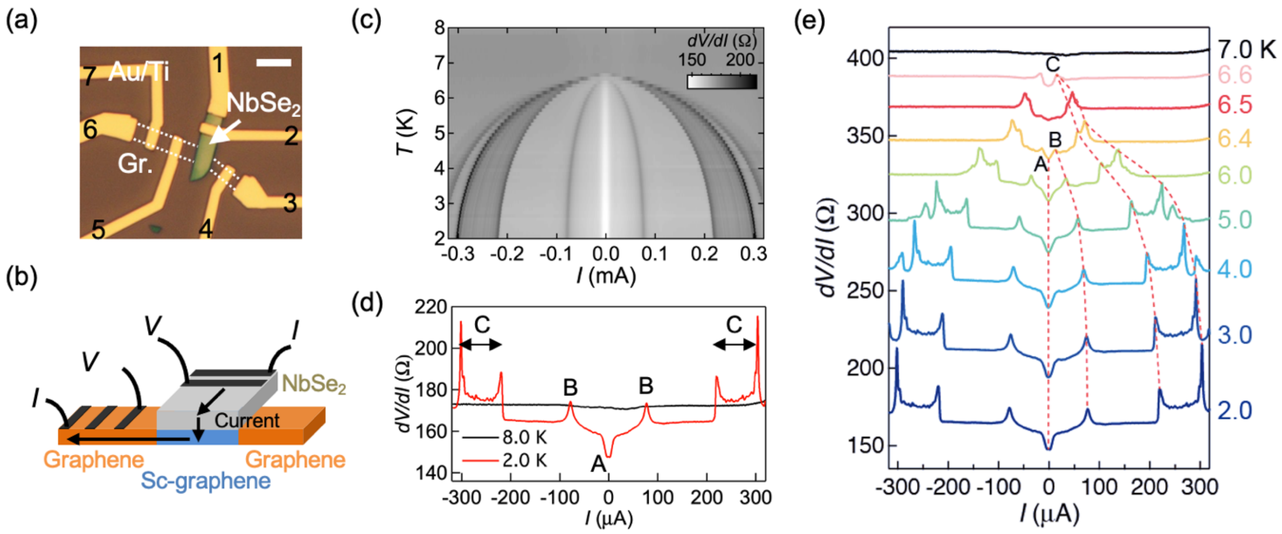

Fig. 1: (a) Optical micrograph of fabricated $NbSe_2$/graphene vdW junction. Scale bar in the figure is 5 μm. (b) Illustration of measurement contact geometry. (c) Image plot for differential resistance dV/dI as a function of dc-current bias I measured in the junction in the temperature range of 2.0 to 8.0 K measured at V_{BG} = −60 V. (d) The dV/dI versus I at 2 K and 8 K. (e) dV/dI versus I at different temperatures. Curves are offset for clarity.